ACS OMEGA

Open Access

This article is licensed under CC-BY-NC-ND 4.0

http://pubs.acs.org/journal/acsodf

Article

Tuning the Microstructures of Electrospray Multicore Alginate Microspheres for the Enhanced Delivery of Astaxanthin

Hongliang Li, Hongjin Yu, Wentao Su, Haitao Wang,* and Mingqian Tan

Cite This: *ACS Omega* 2023, 8, 41537−41547

Read Online

ACCESS | Metrics & More | Article Recommendations | Supporting Information

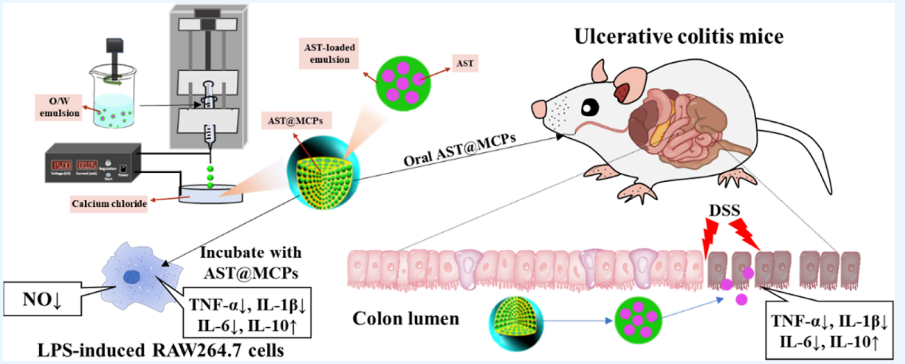

ABSTRACT: Multicore alginate microspheres (MCPs) have been demonstrated as promising carriers for bioactive substances. Herein, the influence of the size of the inner core on the bioaccessibility of astaxanthin (AST) was investigated using both in vitro and in vivo methods. MCPs with different inner core sizes were fabricated in which the oil-in-water emulsion with different oil droplet sizes was embedded in alginate microspheres (AST@MCPs) via the electrospray technology. The AST@MCPs appeared as a uniform sphere with an average size of 300 μm. The AST encapsulation efficiency in the AST@MCPs was determined to be more than 68%, which was independent of the inner core size. The bioaccessibility of AST increased from 38.3 to 83.2% as the size of the inner core decreased. Furthermore, the anti-inflammatory activity of AST@MCPs after in vitro simulated digestion was evaluated by LPS-induced RAW264.7 cells. The results suggested that AST@MCPs with a smaller inner core size exhibited a stronger anti-inflammatory activity, which further proved the results obtained from in vitro simulated digestion. As expected, the oral administration of AST@MCPs significantly mitigated colitis symptoms in DSS-induced ulcerative colitis mice. Compared with AST@MCPs with larger inner cores, AST@MCPs with smaller inner cores reflect stronger anti-inflammatory activity in vivo. These results suggested that the bioaccessibility of AST in MCPs increased significantly with the decrease in the inner core size, which may be attributed to the rapid formation of micelles in the intestine. This work provides a simple and efficient strategy to prepare microspheres for the enhanced delivery of AST, which has important implications for the design of health-promoting foods.

1. INTRODUCTION

Astaxanthin (AST) is a type of lipid-soluble pigment with a range of health benefits, including anti-inflammatory and antioxidant activity.[1,2] However, the poor stability and water-insolubility nature of AST limit its application in the food industry. On the one hand, the conjugated double bonds in the AST were sensitive to the environment's factors (such as temperature), which resulted in extensive degradation during food processing or storage. On the other hand, the poor water solubility of AST led to low bioaccessibility during digestion. Therefore, the development of a delivery system that improves the stability and bioaccessibility of AST is urgently needed.

Recently, oil in water emulsions have been regarded as effective carriers for delivering hydrophobic nutrients. The structure of the emulsion, especially the size of the droplets, significantly influences the bioaccessibility and stability of hydrophobic bioactive substances. Generally, reducing the size of oil droplets helps to improve the accessibility of bioactive substances, thereby increasing their bioaccessibility. This can be attributed to the larger area of the oil−water interface of emulsions with smaller oil droplets, which facilitates oil digestion and micelle formation and therefore improves bioaccessibility. For example, the bioaccessibility of fat-soluble vitamin E increased more than 3-fold when the size of the oil droplet was reduced from 11 to 0.15 μm.[3] Similarly, when the oil droplets were reduced from 9 to 6 μm, the bioaccessibility

Received: July 29, 2023
Revised: September 20, 2023
Accepted: October 12, 2023
Published: October 27, 2023

ACS Publications

© 2023 The Authors. Published by American Chemical Society

of AST loaded in the emulsion increased from 12 to 22%.[4] However, the negative correlation between the size of oil droplets and the bioaccessibility of bioactive substances is not always valid. The high specific surface area of small oil droplets also promotes the contact of sensitive bioactive compounds with the external environment, leading to their degradation and, thereby, lowering their bioaccessibility. For instance, the in vivo experiments suggested that curcumin in nanoemulsion with 100 nm oil droplets has a higher bioaccessibility than that in nanoemulsion with 50 nm oil droplets.[5] On the other hand, the variation in oil droplet size during digestion in the gastrointestinal tract must be taken into account. Coalescence or flocculation may occur before the oil droplets are exposed to lipase in the small intestine. As a result, the oil droplets' size was larger than that in the original emulsion when entering the small intestine and therefore led to a lower bioaccessibility.[6] Consequently, considering the size of oil droplets after oral and gastric digestion rather than their initial size is important, especially when improving bioaccessibility is the goal.

Alginate microspheres have proved their advantages in the delivery of active substances, such as odor taste masking, sensitive ingredients protection, and controllable release of bioactive substances.[7] The calcium alginate network in alginate microspheres is an effective barrier that protects sensitive ingredients from degradation. For example, alginate microspheres were used to deliver betacyanins, which significantly improved the stability of betacyanins during storage.[8] Similarly, the AST embedded in alginate-based carriers showed enhanced stability and bioaccessibility.[9−11] Moreover, the gel network of alginate microspheres exhibited pH-responsive properties, which are stable under acidic conditions and expand in alkali solution.[12] The pH-responsive nature of sodium alginate microspheres enables the intestinal-target release of the nutrients that are encapsulated in them. Therefore, the encapsulation of oil droplets in the network of alginate can improve the stability of lipid-soluble active substances while avoiding the aggregation of oil droplets in the mouth or stomach, thus improving bioaccessibility.

The dripping method is a regularly used technique to fabricate alginate microspheres for encapsulation applications. In this procedure, the alginate solution is added to the gelling solution (such as calcium chloride) dropwise. The size of alginate microspheres obtained by this method is relatively large (greater than 1 mm) and the structure is usually inhomogeneous.[13,14] The large alginate microspheres are difficult to swallow, which limits their application.[15] Therefore, the development of smaller alginate microspheres is critical for their application in food. Electrospraying is a simple method for the fabrication of microspheres that has been widely applied in the food industry.[16,17] Alginate microspheres of a suitable size, which are used to encapsulate bioactive compounds, can be produced using the electrospraying technique. Electrosprayed alginate microspheres with millimeter-sized core−shell structures have been developed for the delivery of fish oil,[18] which achieved the sustained release of nutrition. Alginate microspheres prepared by electrospray technology can also increase the bioaccessibility of β-carotene and hydrophobic polyphenols.[19,20] These results suggest that electrospray technology is a promising method for the preparation of alginate microspheres.

In this study, novel AST-loaded multicore alginate microspheres (AST@MCPs) were fabricated via electrospray methods. In brief, AST was encapsulated within oil-in-water emulsions of different droplet sizes, followed by the incorporation of these droplets into the alginate network through electrostatic spraying. The influence of the inner core size of AST@MCPs on the bioaccessibility of AST was investigated using both in vitro and in vivo methods. Moreover, the anti-inflammatory activity of AST@MCPs was evaluated after in vitro digestion using LPS-induced RAW264.7 cells. For in vivo experiments, the AST@MCPs were fed to a dextran sulfate sodium (DSS)-induced ulcerative colitis mice model. Accordingly, the intervention effect of AST@MCPs was evaluated.

2. MATERIALS AND METHODS

2.1. Materials. Astaxanthin was obtained from Xi'an Realin Biotechnology Co., Ltd. (Xi'an China). Lipopolysaccharide (LPS) was purchased from Beijing Solarbio Science and Technology Co., Ltd. (Beijing, China). Gastric juice and intestinal juice were purchased from Shanghai Yuanye Biotechnology Co., Ltd. (Shanghai, China). DSS was bought from Yeasen Biotechnology Co., Ltd. (Shanghai, China). The liquid feed was purchased from Trophic Animal Feed High-tech Co., Ltd. (Jiangsu, China). The test kits for nitric oxide (NO), myeloperoxidase (MPO), inducible nitric oxide synthase (iNOS), maleic dialdehyde (MDA), reduced glutathione (GSH), catalase (CAT), superoxide dismutase (SOD), interleukin-10 (IL-10), tumor necrosis factor (TNF-α), interleukin-6 (IL-6), and interleukin-1β (IL-1β) were obtained from Nanjing Jiancheng Bioengineering Institute Co., Ltd. (Nanjing, China).

2.2. Preparation and Characterization of Emulsion and Alginate Microspheres. AST was fully dissolved in edible soybean oil (2 mg mL^{-1}) by stirring for 24 h and was used to prepare AST@MCPs. The MCPs are prepared by a two-step method. The oil-in-water emulsions with various oil droplet sizes were prepared by a combination of high-speed homogenization and high-pressure homogenization methods. The oil-in-water emulsions with large oil droplets (13 μm) were obtained by homogenizing the mixture of 40 mL saponin solution (1.5%) and 10 mL soybean oil via a high-speed disperser (10,000 rpm, 5 min, IKA, Staufen, Germany). For emulsions with 1 μm oil droplets, a higher homogeneous speed (15,000 rpm) was applied. The emulsion with large oil droplets was homogenized by a high-pressure homogenizer (Avestin, Ottawa, Canada) at 500 bar for three cycles and the size of oil droplets was reduced to 0.34 μm. The emulsions with the smallest oil droplet size were prepared by homogenizing the emulsions with large oil droplets at 1000 bar for three cycles. The morphology of water-in-oil emulsions with varying droplet sizes was examined using an optical microscope (Nikon, Tokyo, Japan). The size distribution of the emulsions was determined by diluting them 1000-fold and analyzing them with a laser particle size analyzer (Malvern Panalytical, Malvern, UK).

The sodium alginate solution was mixed with as-prepared emulsions in a ratio of 1:5 (v/v), and the MCPs were obtained by an electrospray device. The electrospray device consists of a high-voltage direct current power supply (0−30 kV from the emitter to the collector) and a stepper motor controller (Four-Dimensional, Beijing, China). The voltage was adjusted between 0 and 20 kV, and the distance from the spray needle tip to the calcium chloride solution was varied from 2 to 10 cm. The calcium chloride solution was contained in a circular dish with a diameter of 9 cm. The solution advancing speed

https://doi.org/10.1021/acsomega.3c05542
ACS Omega 2023, 8, 41537−41547

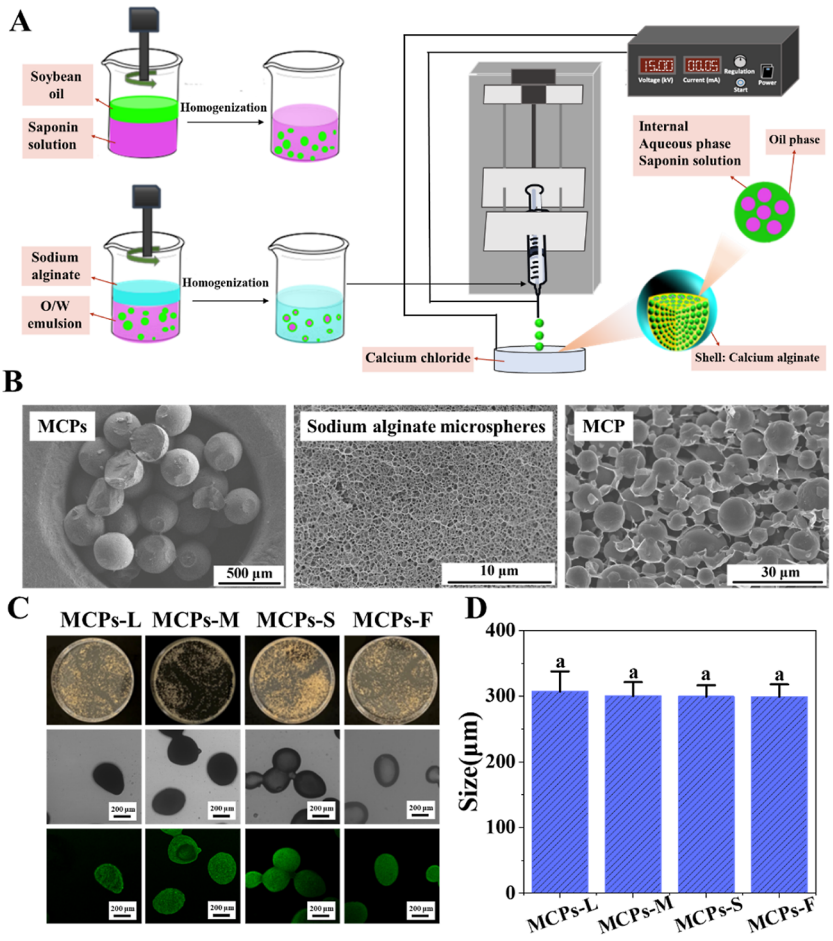

Figure 1. Preparation and characterization of electrosprayed MCPs. Schematic illustration of the preparation of MCPs (A). The Cryo-SEM images depict the external structure of MCPs, the internal structure of sodium alginate microspheres, and the internal structure of MCPs (B). Appearance and confocal microscopy images of MCPs (C). The diameter of MCPs with different inner oil droplet sizes (D). MCPs-L: MCPs with large oil droplets, MCPs-M: MCPs with medium oil droplets, MCPs-S: MCPs with small oil droplets, and MCPs-F: MCPs with fine oil droplets. Samples with significant ($p < 0.05$) differences were labeled with different lowercase letters.

was set between 20 and 80 μL s^{-1}, and the concentration of sodium alginate solution ranged from 0.5 to 3%. The microstructures of MCPs were characterized by using a scanning electron microscope (Hitachi, Tokyo, Japan) equipped with a Cryo-SEM preparation system (Quorum, PP3010T, Lewes, UK). MCPs were characterized using a confocal laser scanning microscope (Leica, Weztlar, Germany), with the oil phase labeled with 100 μmol L^{-1} Nile red (excitation wavelength: 488 nm, emission wavelength: 580 nm).

2.3. Encapsulation Efficiencies and AST Loading of AST@MCPs. The AST in the AST@MCPs was extracted by ethanol. Briefly, 0.05 g of AST@MCPs was placed in a centrifuge tube with 2 mL of ethanol; the mixture was subjected to sonication for a duration of 30 min, and the supernatant was collected by centrifugation (7000 rpm, 10 min). The concentration of AST in the supernatants was assessed by measuring the absorbance at 478 nm. The loading capacity and encapsulation efficiency were calculated according to eqs 1 and 2.

$$\text{Loading capacity (\%)} = \frac{M_{AST}}{M_0} \times 100\% \quad (1)$$

$$\text{Encapsulation efficiency (\%)} = \frac{M_{AST}}{M_1} \times 100\% \quad (2)$$

where M_{AST} is the weight (mg) of astaxanthin in AST@MCPs, M_0 is the weight (mg) of MCPs, and M_1 is the weight (mg) of astaxanthin that is used for preparing AST@MCPs.

2.4. In Vitro Digestion of AST@MCPs. Simulated in vitro digestion of AST@MCPs was performed at 37 °C. The procedure was according to the previously reported method.[21] 100 mg samples were blended with 4 mL of simulated gastric juice (2.0 g L^{-1} NaCl, 3.2 g L^{-1} gastric pepsin, the pH was adjusted to 1.2 by using HCl) and incubated for 2 h. Subsequently, the pH value of the mixture was adjusted to 7.5 before adding 4 mL of artificial intestinal fluid (6.8 g L^{-1} potassium dihydrogen phosphate, 10 g L^{-1} pancreatin, and the pH was adjusted to 6.8 by using NaOH).

The release profile of AST in AST@MCPs during the in vitro digestion process was evaluated by the previous method.[22] During in vitro digestion, the undigested oil phase floated in the upper layer of the digest due to its low density. To determine the released AST in the digest, 1 mL of the digest below the oil layer was taken and the AST was extracted by an equal volume of extract agent (methanol/dichloromethane = 1:1). The astaxanthin content was calculated according to the method described in Section 2.3.

https://doi.org/10.1021/acsomega.3c05542
ACS Omega 2023, 8, 41537−41547

The mixture after in vitro digestion was centrifuged at 15,000 g for 40 min, and the micelle layers were obtained. The AST content in the micelle layers was determined following extraction using an equal volume of extraction agent (methanol/dichloromethane = 1:1). The bioaccessibility of AST was calculated according to eq 3

$$\text{bioaccessibility}\ (\%) = \frac{C_M}{C_T} \times 100\% \quad (3)$$

where C_M is the amount (mg) of AST in the micelle fraction and C_T is the total amount of AST (mg).

2.5. In Vitro Anti-Inflammatory. The in vitro anti-inflammatory ability of AST@MCPs was evaluated by LPS-induced RAW264.7 cells, following the previously described methodology.[23] Briefly, RAW264.7 cells were cultured in six-well plates at a seeding density of 1×10^5 cells/well and allowed to grow for 24 h. The cells were exposed to LPS for a duration of 24 h to induce an inflammatory reaction. After being treated with free AST (20 μg mL^{-1}), AST-loaded emulsions (50 μg mL^{-1}, equivalent to 20 μg mL^{-1} AST), and AST@MCPs (4 mg mL^{-1}, equivalent to 20 μg mL^{-1} AST) for 24 h, the levels of NO, TNF-α, IL-1β, IL-6, and IL-10 were determined by biochemical kits. To investigate the effect of digestion on the anti-inflammatory capacity of the testing samples, samples were subjected to in vitro digestion (the amount of sample used for in vitro digestion was identical to that used in the anti-inflammatory assay), and micelle layers obtained from the mixtures after in vitro digestion were added to the culture medium. The levels of NO, TNF-α, IL-1β, IL-6, and IL-10 were measured to evaluate the anti-inflammatory ability.

2.6. In Vivo Intervention of AST@MCPs against Colon Colitis in Mice. The male BALB/c mice (specific pathogen-free, SPF) of 6−8 weeks were obtained from Liaoning Changsheng Biotechnology Co., Ltd. and housed under the laboratory environment (12 h light−dark cycle each day, the temperature was 23 ± 2 °C, and the relative humidity from 40 to 60%). The liquid feed was readily available throughout the duration of the study. The mice were assigned to five groups (n = 8) through a random allocation process: control group, model group (DSS), astaxanthin group (AST), AST@MCPs with large oil droplets group (AST@MCPs-L), and AST@MCPs with fine oil droplets group (AST@MCPs-F). The dosage of AST was 25 mg/kg/day, and the amount of AST@MCPs was calculated based on their loading capacity. AST and AST@MCPs were added to the liquid feed. The DSS-induced colon colitis in mice was established following the previous method.[24−26] After 14 days, 3% DSS was added to the liquid feed for all groups except the control group. After a period of 4 days, the mice were euthanized, and serum and organs were collected for further analysis. The levels of SOD, CAT, MDA, MPO, iNOS, and GSH in the colon were measured. Inflammatory factors, such as IL-10, IL-6, IL-1β, and TNF-α in serum, were measured. The animal experiments were carried out in accordance with the regulations established by the Institutional Animal Ethics Committee (DLPU2021037) of Dalian Polytechnic University, and the authors of this study ensured that all ethical regulations were adhered to throughout the research process.

2.7. Statistical Analysis. The data were reported as mean ± standard deviation. Statistical analysis was carried out utilizing SPSS25, and the significance of the data was determined through one-way analysis of variance (ANOVA). $p < 0.05$ was regarded as statistically significant.

3. RESULTS AND DISCUSSION

3.1. Preparation of Electrospray MCPs. The preparation of MCPs involved a two-step method, as illustrated in Figure 1A. First, oil-in-water emulsions were prepared with saponin as the emulsifier, and then, the electrospraying jet solution was obtained by mixing the oil-in-water emulsion and sodium alginate solutions. Second, jet solutions were sprayed into the collecting solutions that contained calcium chloride by a custom-designed electrospray device and MCPs were formed via ionic gelation. To reveal the multicore structure of MCP, cryoscanning electron microscopy was employed (Figure 1B). MCPs exhibited spherical shapes with a diameter of approximately 300 μm. In the absence of an emulsion, sodium alginate microspheres displayed a typical network structure in the cross-section. However, in the case of MCP, oil droplets were distributed within the sodium alginate network, resulting in a multicore structure.

3.2. Tuning the Microstructures of AST@MCPs. AST is a superior antioxidant, with various beneficial effects on human health. Therefore, AST was chosen as a model substance to evaluate the carrier ability of MCPs. For an electrospraying process, the jet solution was sprayed from the tip of the needle and formed stable droplets under an electric field. The gelation occurred when the droplets of jet solution entered into the collecting solutions, and many factors, such as the strength of the electric field, the distance between the needle and collecting solutions, and the concentrations of sodium alginate, affect the properties of the microspheres. Thus, the effects of the preparation conditions on the morphology of MCPs were carried out.

The electrostatic strength played a vital role in determining the formation process of the alginate microspheres. The size of the alginate microspheres decreased with the increase in voltage, which could be attributed to the greater drawing force generated by the larger voltages.[16] The diameter of alginate microspheres reached its minimum (310 μm) when the voltage was 15 kV and remained unchanged as the voltage continued to increase (Figure S1A). The effects of the distance between the needle and the surface of the calcium chloride solutions on MCPs were investigated. A tailing phenomenon was observed when the distance was 10 cm. The MCPs exhibited a spherical appearance with a decrease in distance. However, a distance shorter than 7 cm was not conducive to the formation of MCPs, since their size became uneven, which could be attributed to an arc discharge phenomenon.[27] The flow rate affected the size of the MCPs as well. When the flow rate was greater than 40 μL s^{-1}, MCPs with regular appearance could not be obtained. The gelation rate of alginate was low when the concentration of sodium alginate was less than 1%, and the oil droplets were transported into collecting solutions before being fixed in the MCPs. Therefore, the calcium chloride solutions became turbid, and cylindrical MCPs were obtained. When the sodium alginate concentration exceeded 3%, the size of the MCPs became large, which could be attributed to the high viscosity. Therefore, the optimized conditions for the preparation of MCPs were as follows: the alginate concentration was 2%, the flow rate was 40 μL s^{-1}, the voltage was 15 kV, and the height between the surface of collecting solutions and the needle was 7 cm (Figure S1A).

https://doi.org/10.1021/acsomega.3c05542
ACS Omega 2023, 8, 41537−41547

The MCPs with different microstructures were prepared by changing the droplet size in the oil-in-water emulsion. Emulsions with different oil droplet sizes were obtained using various homogenization methods: emulsion with large oil droplets (diameter of 13 μm); emulsion with medium oil droplets (diameter of 1 μm); emulsion with small oil droplets (diameter of 0.34 μm); and emulsion with fine oil droplets (diameter of 0.29 μm). The four emulsions exhibited a single-peak distribution of oil droplet sizes (Figure S1B). MCPs loaded with different emulsions were prepared by the electrospray method under the optimized condition. The morphology of the MCPs was spherical, and their microstructures were observed by confocal microscopy after being stained with Nile red. Green signals were evenly distributed within the MCPs (Figure 1C), suggesting the oil droplets were encapsulated in the MCPs effectively. The diameters of MCPs prepared with different emulsions (MCPs-L, MCPs-M, MCPs-S, and MCPs-F) were similar, approximately 300 μm (Figure 1D). This finding indicates that the morphology of the MCPs remained unaffected by the size of oil droplets in the emulsion but was only related to the conditions applied in electrospray.

3.3. In Vitro Digestion of AST@MCPs. The AST-loaded MCPs (AST@MCPs) prepared from emulsions with different oil droplet sizes (13, 1, 0.34, and 0.29 μm) were designated as AST@MCPs-L, AST@MCPs-M, AST@MCPs-S, and AST@MCPs-F, respectively. The effects of the oil droplet size on loading performance were investigated. The encapsulation efficiency of AST in the MCPs was 68% (Figure 2A).

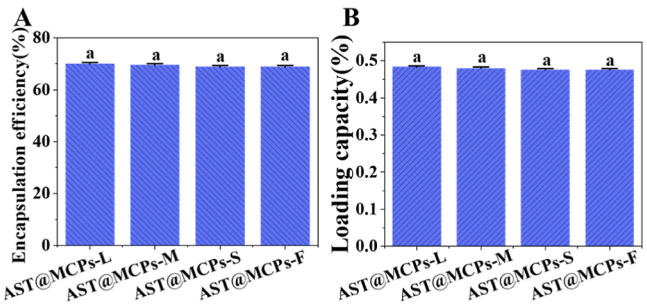

Figure 2. Encapsulation efficiency (A) and loading capacity (B) of AST@MCPs with different inner core sizes. AST@MCPs-L: AST@MCPs with large oil droplets, AST@MCPs-M: AST@MCPs with medium oil droplets, AST@MCPs-M: AST@MCPs with small oil droplets, and AST@MCPs-F: AST@MCPs with fine oil droplets. Samples with significant ($p < 0.05$) differences were labeled with different lowercase letters.

Compared to the encapsulation efficiency of 63.9 ± 3.0% achieved using the ionic gelation method to prepare chitosan-tripolyphosphate nanoparticles for AST delivery, AST@MCPs are more favorable for the encapsulation of AST.[28] At the same time, the loading capacity of AST in the MCPs was measured to be 0.47% (Figure 2B). The astaxanthin nanocapsules prepared using β-cyclodextrin, decapolyglycerol monooleate, and soybean lecithin as shell materials via high-pressure homogenization have a loading capacity of approximately 0.54%,[29] which is similar to the loading capacity of AST@MCPs. These results revealed that the MCPs were suitable for embedding AST and that the size of oil droplets had a negligible effect on the encapsulation of AST in MCPs.

The release profile of AST in the MCPs with different oil droplets during digestion was investigated. The appearance of AST@MCPs at different digestion stages during in vitro digestion is shown in Figure 3A. Most of the AST@MCPs maintained the spherical state in the stomach juices at the initial stage. The high stability of AST@MCPs in stomach juices could be attributed to the high-stability nature of calcium alginate in an acidic environment. AST@MCPs-L was partially destroyed by the increase in incubation time since the oil droplets were released from the MCPs and aggregated into large oil droplets. The relatively low stability of AST@MCPs-L could be attributed to their loose structure, as the large oil droplets weaken the gel strength of sodium alginate. The AST@MCPs cracked after being transferred to the simulated intestinal fluid. The molecular chains of sodium alginate stretched with the increase of the pH value, led to the disintegration of microspheres.[30,31] The oil droplets inside the alginate microspheres were completely released in the simulated intestinal fluid and favored the absorption of AST dissolved in the oil phase.

Furthermore, the AST release profile of AST@MCPs with different inner oil droplet sizes was investigated during in vitro digestion. AST in AST@MCPs was mainly released in the intestinal fluid since the AST contents in the intestinal fluid were significantly higher than that in the gastric fluid. This result further confirmed the intestinal targeted release properties of AST@MCPs. Moreover, the size of the inner oil droplets played an essential role in the AST release of AST@MCPs. When the AST@MCPs with large oil droplets were digested by stomach fluid, the content of AST in stomach juices was 0.17 mg mL^{-1}, which was significantly higher than that with smaller inner oil droplets. On the contrary, the AST release amount in the intestinal fluid was negatively correlated with the size of inner oil droplets of AST@MCPs. The highest AST content of 0.78 mg mL^{-1} was achieved when AST@MCPs-F was digested by intestinal fluid. Furthermore, the bioaccessibility of AST embedded in AST@MCPs was determined. As shown in Figure 3C, the bioaccessibility of AST dissolved in soybean oil was 8.28%, consistent with the low bioaccessibility typically observed for lipophilic compounds in oil.[32] However, after encapsulation within emulsions and AST@MCPs, the bioaccessibility of AST significantly increased. The highest bioaccessibility of 83.20% was observed in AST@MCPs-F as expected, which indicated that decreasing the size of inner oil droplets can effectively improve the bioaccessibility of the AST. Previous investigations yielded comparable findings, where carotenoid bioaccessibility increased with the decrease in lipid droplet size in corn oil-in-water emulsions.[33]

Generally, the size of the droplets in the emulsion played an essential role in the bioaccessibility of hydrophobic bioactive compounds embedded in emulsions. The enhanced bioaccessibility of hydrophobic bioactive compounds in emulsions with small oil droplet sizes can be attributed to the fact that small oil droplets facilitate oil digestion and micelle formation. Notably, micelles form in the small intestine; therefore, the droplet size of the emulsion upon reaching the small intestine is more critical for bioaccessibility. Previous results suggested the bioaccessibility of curcumin in nanoemulsion with 100 nm oil droplets was higher than that in nanoemulsion with 50 nm oil droplets.[5] This result could be attributed to the coalescence or flocculation of oil droplets before they were exposed to lipase in the small intestine. For AST@MCPs, the oil droplets of the emulsion were embedded inside the calcium alginate gel by electrospray and formed a multicore structure. Alginate

https://doi.org/10.1021/acsomega.3c05542
ACS Omega 2023, 8, 41537−41547

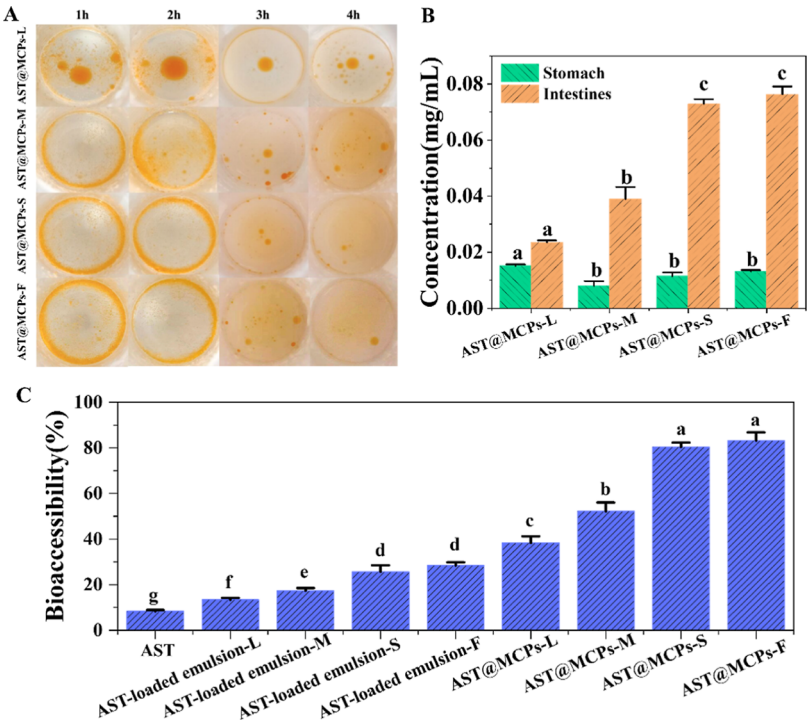

Figure 3. Appearance (A), AST concentration (B), and bioaccessibility (C) of AST@MCPs with different inner core sizes during in vitro simulated digestion. AST: astaxanthin, AST-loaded emulsion-L: AST-loaded emulsion with large oil droplets, AST-loaded emulsion-M: AST-loaded emulsion with medium oil droplets, AST-loaded emulsion-S: AST-loaded emulsion with small oil droplets, AST-loaded emulsion-F: AST-loaded emulsion with fine oil droplets, AST@MCPs-L: AST@MCPs with large oil droplets, AST@MCPs-M: AST@MCPs with medium oil droplets, AST@MCPs-S: AST@MCPs with small oil droplets, and AST@MCPs-F: AST@MCPs with fine oil droplets. Samples with significant ($p < 0.05$) differences were labeled with different lowercase letters.

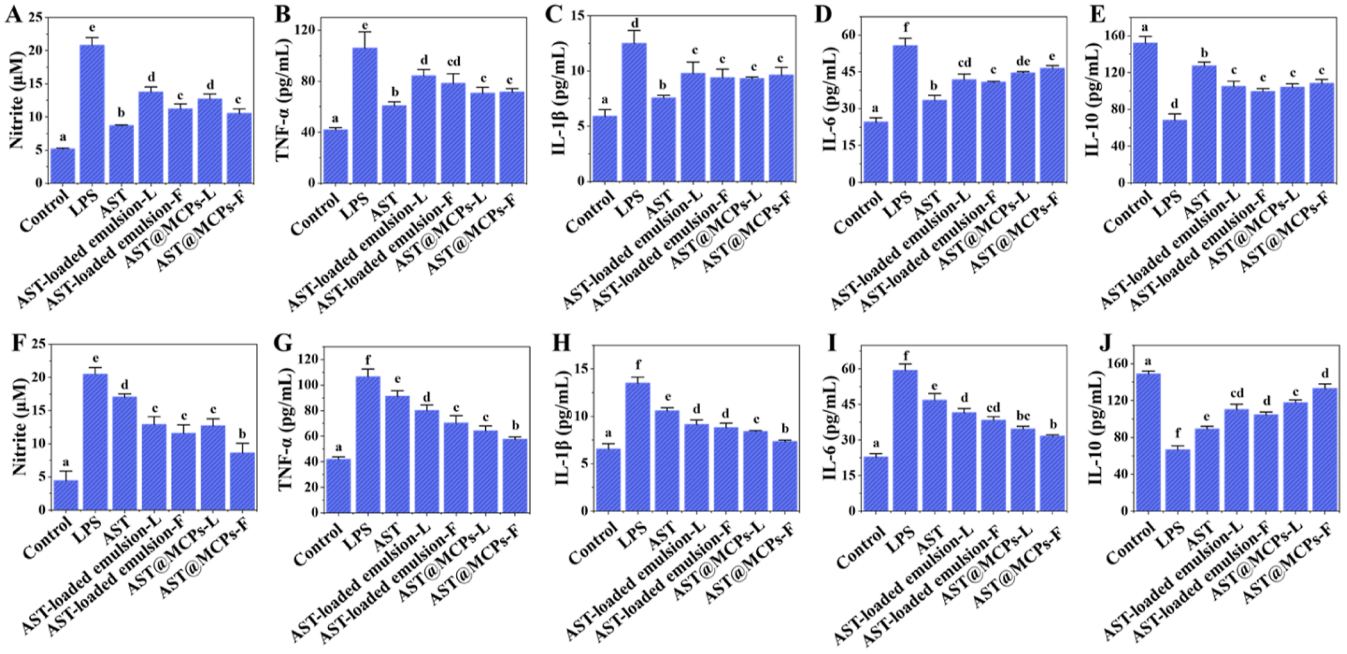

Figure 4. In vitro anti-inflammatory effects of AST@MCPs analyzed by LPS-induced RAW 264.7. The effect of AST-loaded emulsions and AST@MCPs on the inflammation factors level of nitrite (A), TNF-α (B), IL-1β (C), IL-6 (D), and IL-10 (E). The effect of digestive products of AST-loaded emulsion and AST@MCPs on the inflammation factors level of nitrite (F), TNF-α (G), IL-1β (H), IL-6 (I), and IL-10 (J). AST: astaxanthin, AST-loaded emulsion-L: AST-loaded emulsion with large oil droplets, AST-loaded emulsion-F: AST-loaded emulsion with fine oil droplets, AST@MCPs-L: AST@MCPs with large oil droplets, and AST@MCPs-F: AST@MCPs with fine oil droplets. Samples with significant ($p < 0.05$) differences were labeled with different lowercase letters.

microcapsules exhibit pH-responsive release properties that protect oil droplets from aggregating before reaching the intestine, which contributes to the improvement of bioaccessibility. Therefore, reducing the size of oil droplets and

https://doi.org/10.1021/acsomega.3c05542
ACS Omega 2023, 8, 41537−41547

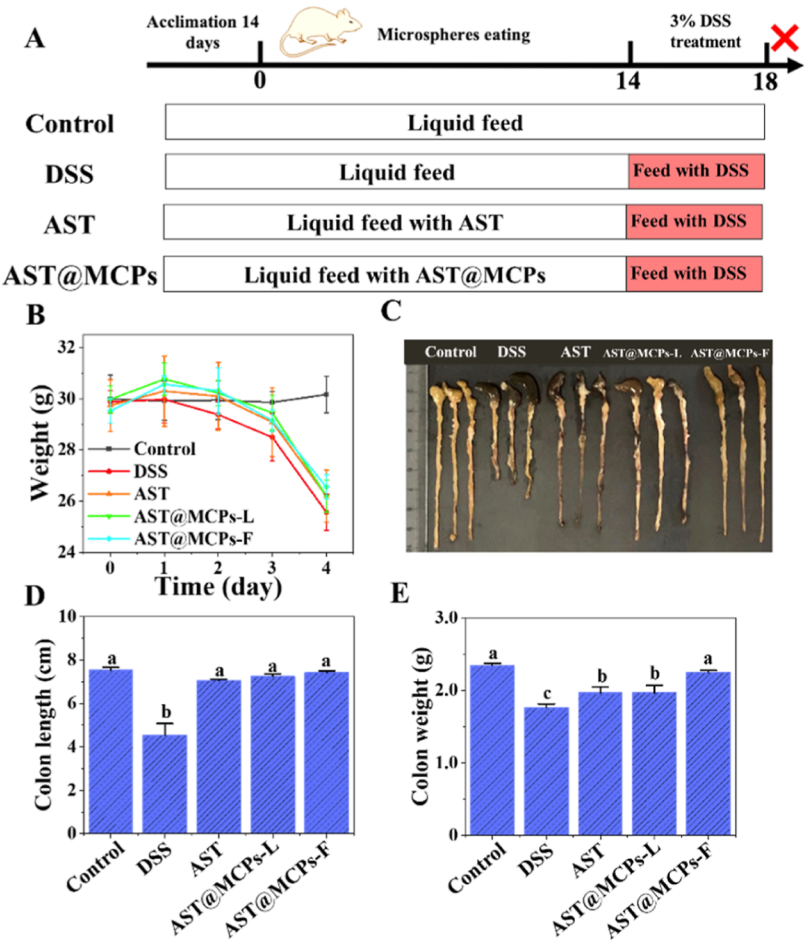

Figure 5. Schematic representation of the in vivo anti-inflammatory activity evaluation assay (A). Changes in body weight (B). Photographs of colons in different groups (C). Colon length in different groups (D). Colon weight in different groups (E). AST: astaxanthin, AST@MCPs-L: AST@MCPs with large oil droplets, and AST@MCPs-F: AST@MCPs with fine oil droplets. Samples with significant ($p < 0.05$) differences were labeled with different lowercase letters.

preventing the aggregation of oil droplets are the main ways for alginate microcapsules to improve astaxanthin bioaccessibility.

3.4. Anti-Inflammatory Activity of AST@MCPs. According to the results obtained from the simulated digestion, the bioaccessibility of AST in AST@MCPs-L was the lowest, while that in AST@MCPs-F was the highest; therefore, these two AST@MCPs were selected as examples to evaluate the anti-inflammatory activity of AST@MCPs. The anti-inflammatory effects of AST@MCPs were evaluated in vitro by measuring the levels of inflammatory indicators in LPS-induced inflammation of RAW264.7 cells.[34] The LPS-induced RAW264.7 cells exhibited significantly increased levels of NO, TNF-α, IL-1β, and IL-6 and significantly reduced levels of IL-10 compared with the control group, indicating that the LPS-induced inflammation model was successfully established (Figure 4A–E). After incubation with free AST, the levels of NO, TNF-α, IL-1β, and IL-6 in the LPS-induced RAW264.7 cells model decreased significantly, while the levels of IL-10 increased significantly, indicating AST can effectively alleviate the inflammation as expected.[35,36] On the contrary, the NO level after incubation with emulsion (irrespective of the size of the oil droplets) or MCPs (irrespective of the size of the oil droplets) were comparable to that in the LPS treatment group (Figure S2), suggesting wall materials have no anti-inflammatory activity. Additionally, the AST-loaded emulsion or AST@MCPs showed significant anti-inflammatory activity.

For oral astaxanthin carriers, the AST embedded in the carriers was exposed to harsh conditions inside the digestive tract before they exerted their anti-inflammatory effects. Therefore, the products of AST, AST-loaded emulsions, and AST@MCPs after in vitro digestion were incubated with LPS-induced RAW 264.7 cells and their anti-inflammatory activity was evaluated (Figure 4F–J). Unlike free AST, the anti-inflammatory activity of AST after in vitro digestion decreased sharply, which could be attributed to the low bioaccessibility of AST. The in vitro digestion products of AST-loaded emulsions exhibited higher anti-inflammatory activity than the digested AST, suggesting the emulsions improved the bioaccessibility of AST. Notably, the anti-inflammatory activity of digested AST@MCPs-F was higher than that with large oil droplets, indicating that the bioaccessibility of AST in AST@MCPs with small oil droplets was higher. This result was in line with the results obtained from the bioaccessibility assay. Additionally, the size of oil droplets had a negligible effect on the anti-inflammatory activity of the digested emulsion, whereas the anti-inflammatory activity of digested AST@MCPs highly depended on the size of inner oil droplets. Therefore, the anti-inflammatory activity of AST@MCPs with smaller oil droplets was high.

https://doi.org/10.1021/acsomega.3c05542
ACS Omega 2023, 8, 41537−41547

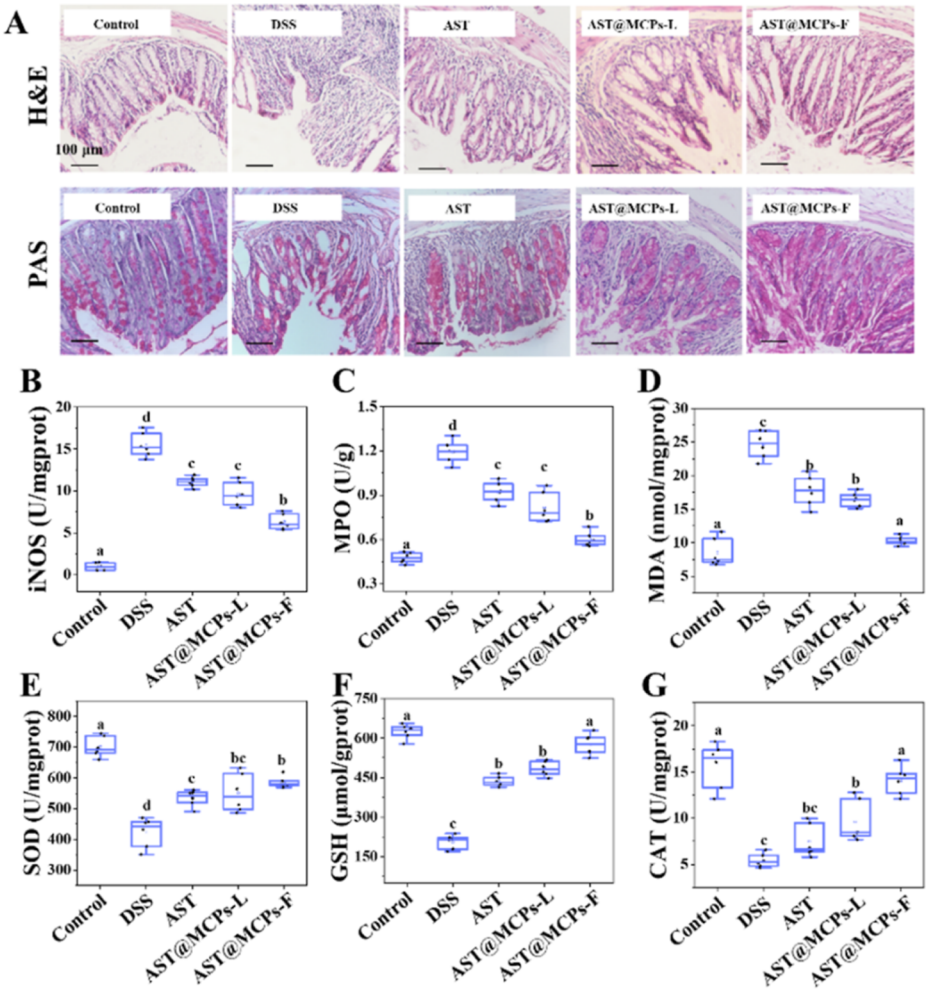

Figure 6. H&E-staining and PAS staining of colon sections in different groups (A). Effects of AST@MCPs on iNOS (B), MPO (C), MDA (D), SOD (E), GSH (F), and CAT (G) in the colon tissue of mice in each group. AST: astaxanthin, AST@MCPs-L: AST@MCPs with large oil droplets, and AST@MCPs-F: AST@MCPs with fine oil droplets. Samples with significant ($p < 0.05$) differences were labeled with different lowercase letters.

3.5. Intervention Effect of AST@MCPs against Colon Colitis in Mice. After demonstrating the in vitro anti-inflammatory activity of AST@MCPs, their intervention effect on DSS-induced ulcerative colitis in mice was evaluated to further prove the inhibitory effects on the inflammatory response in vivo (Figure 5A). The common indicators of colon colitis, such as body weight loss and colon length, were determined. As the extension of the DSS treatment continued, mice experienced rapid weight loss. On the fourth day after DSS administration, the mice in the DSS-treated group showed a significant reduction in body weight, with a decrease of 4.60 g compared to the control group. The presence of AST alleviated DSS-induced weight loss in mice. In the free AST, AST@MCPs-L, and AST@MCPs-F groups, body weight of mice decreased by 3.88, 3.86, and 3.61 g, respectively (Figure 5B). The results showed that AST@MCPs had the best intervention effect on weight loss caused by DSS-induced colon colitis.[37] The length of the colon reflects the degree of colon inflammation and it is negatively correlated with the inflammatory injury.[11] Subsequently, the colons of mice were collected, and their length was measured (Figure 5C−E). In the DSS group, the colon length was measured to be 4.53 ± 0.67 cm, which showed a significant decrease in length compared to the control group. Moreover, congestion and swelling of the colon were observed in the DSS-treated group, which further illustrated the severity of inflammation. Oral administration of free AST, AST@MCPs-L, and AST@MCPs-F alleviated the colonic shortening symptoms as expected. The colon length in these groups was significantly longer than that in the DSS group. Among them, the longest average colon was obtained in the AST@MCPs-F treated group (7.42 ± 0.10 cm), indicating their high anti-inflammation activity. Colon weight showed a similar trend to colon length, which obtained similar conclusions. These results demonstrated that the inner oil droplets' size of AST@MCPs affected the bioaccessibility of AST and subsequently the anti-inflammation activity in vivo.

In addition, to investigate the pathological alterations in colon tissues, mouse colon were subjected to histological examination using H&E and PAS staining methods after being treated with free AST, AST@MCPs-L, and AST@MCPs-F.[38,39] As depicted in Figure 6A, in the control group, the colonic mucosa appeared intact without any evidence of ulcer formation or infiltration of the inflammatory cells. In DSS-treated group, the colon tissues were seriously damaged. Compared with the healthy control group, ulceration and erosion occurred in the colonic mucosa of DSS-induced mice. Moreover, the glandular morphology of epithelial cells and lamina propria was seriously damaged. At the same time, the

https://doi.org/10.1021/acsomega.3c05542
ACS Omega 2023, 8, 41537−41547

goblet cells were significantly reduced, and the crypt structure was destroyed. Many inflammatory cells were observed within both the mucosal layer and submucosa of the colon. The damage caused by DSS was alleviated after intervention with free AST, AST@MCPs-L, and AST@MCPs-F. Notably, AST@MCPs-F almost completely alleviated the inflammation in the colon tissue since the histological structure of the colon in the AST@MCPs-F treated group was similar to that in the control group. The high anti-inflammatory activity of AST@MCPs with fine oil droplets could be attributed to their high bioaccessibility, which delivers more AST to the site of inflammation. In addition, the histological structures of the lung, stomach, heart, spleen, kidney, liver, and testis were characterized as well, and no significant differences were observed in these tissues (Figure S3), suggesting the high biocompatibility of AST@MCPs.

The activity of inflammation-related enzymes (iNOS and MPO) in the colon was determined. iNOS increased significantly in the inflammation tissues and produced NO until the cells were degraded. MPO mainly exists in neutrophils and monocytes[40] and acts as a mediator in the process of inflammatory response. MPO activity correlated positively with the inflammation severity. After treatment with DSS, the activity of iNOS and MPO in the colon exhibited a significant increase when compared to that of the control group. Administration of free AST or AST@MCPs attenuated the increase in the MPO and iNOS activity in DSS-induced colitis. Moreover, the best alleviation effect was achieved with the administration of AST@MCPs-F, suggesting the highest in vivo anti-inflammation activity.

Oxidative stress occurs when the imbalance between antioxidants and oxidation was destroyed. Inflammation in ulcerative colitis is associated with oxidative stress since the level of oxygen species in the colon was more than 10 times that in healthy individuals.[41] The elevated levels of reactive oxygen species stimulate inflammatory mediator production, contributing to inflammation. Therefore, the oxidative stress markers (SOD, CAT, MDA, and GSH) in colon tissue were determined to evaluate the intervention effects of AST@MCPs. In Figure 3D−F, the levels of GSH showed a dramatic decline, while the levels of MDA markedly increased in the DSS-treated group. At the same time, the activity of CAT and SOD in the DSS-treated group was low compared to that in the control group. Those results demonstrated that DSS treatment leads to oxidative stress in the colon as described previously.[26] Interestingly, AST, AST@MCPs-L, and AST@MCPs-F reduced the MAD levels in the DSS-treated mice. The activity of SOD and CAT was enhanced in those groups as well. As expected, AST@MCPs-F exhibited the best intervening effect among those treatments. The results indicated that AST@MCPs-F relieves DSS-induced oxidative stress in vivo.

The effects of AST@MCPs on pro-inflammatory and anti-inflammatory factors in blood were determined (Figure 7). In the DSS group, the levels of TNF-α, IL-1β, and IL-6 in the blood of mice markedly increased when compared with the control group, indicating the presence of severe inflammatory reactions. After intervention with AST@MCPs, the levels of TNF-α, IL-6, and IL-1β exhibited a significant decrease compared to the DSS group, among which, the level of TNF-α, IL-1β, and IL-6 in the AST@MCPs treated group was the lowest, indicating that AST@MCPs effectively reduced the DSS-induced pro-inflammatory response. On the contrary, IL-10, the anti-inflammatory cytokine, shows an opposite trend to those proinflammatory cytokines. The IL-10 level in the DSS group exhibited a significant decrease, indicating that severe inflammatory reactions occurred.[42] Compared with the DSS group, AST and AST@MCPs treatment improved the level of IL-10, which further proved their anti-inflammatory activity. These results suggested that AST@MCPs with a smaller inner core size effectively improve the bioaccessibility of active ingredients,[43] which had better anti-inflammatory effects and alleviate ulcerative colitis in vivo.

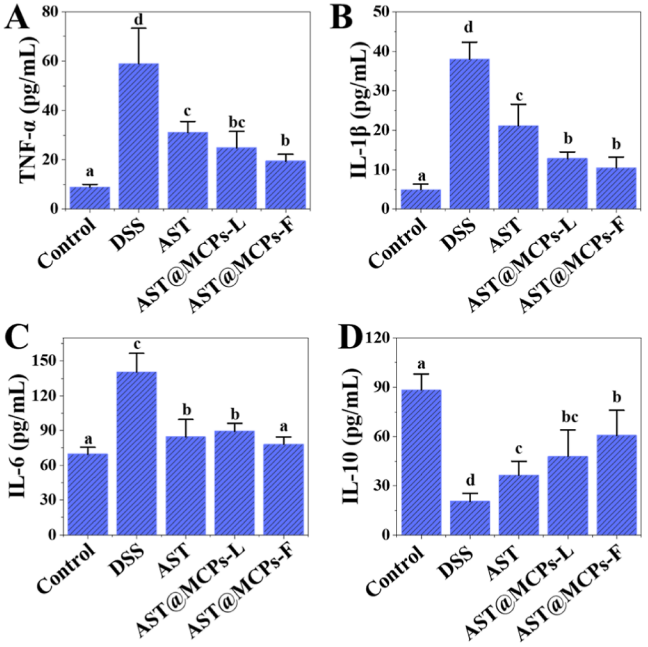

Figure 7. Levels of TNF-α (A), IL-1β (B), IL-6 (C), and IL-10 (D) in the blood serum of mice in each group. AST: astaxanthin, AST@MCPs-L: AST@MCPs with large oil droplets, and AST@MCPs-F: AST@MCPs with fine oil droplets. Samples with significant ($p < 0.05$) differences were labeled with different lowercase letters.

4. CONCLUSIONS

In summary, AST@MCPs with different inner core sizes were fabricated with electrospray technology. The in vitro digestion proved the intestinal targeting properties of AST@MCPs. Furthermore, the effects of the inner core size on the AST bioaccessibility were investigated by using both in vitro and in vivo methods. The inner core size of AST@MCPs has a significant effect on the bioaccessibility of AST. A 2-fold increase in AST bioaccessibility was observed when the inner core sizes decreased from 13 to 0.29 μm. Additionally, the high AST bioaccessibility was also proved by the high anti-inflammatory activity of AST@MCPs with a small inner core size by using the LPS-induced RAW264.7 cell model. Moreover, the AST@MCPs-F effectively alleviated the DSS-induced damage in the colon, which demonstrated their high bioaccessibility in vivo. The results obtained confirmed that MCPs were a promising carrier for the delivery of AST and provided valuable information for the design of health-promoting nutraceutical foods.

https://doi.org/10.1021/acsomega.3c05542
ACS Omega 2023, 8, 41537−41547

■ ASSOCIATED CONTENT

Supporting Information

The Supporting Information is available free of charge at https://pubs.acs.org/doi/10.1021/acsomega.3c05542.

Topography of MCPs prepared under different conditions, microscopic images and oil droplets size distribution of emulsion, anti-inflammatory effect of emulsion and MCPs, and pathological sections of various organs in mice (PDF)

■ AUTHOR INFORMATION

Corresponding Author

Haitao Wang − *State Key Lab of Marine Food Processing & Safety Control, Dalian Polytechnic University, Dalian 116034 Liaoning, China; National Engineering Research Center of Seafood, Collaborative Innovation Center of Seafood Deep Processing, Nutrition and Health Food Pilot Base of Liaoning Dalian, and Academy of Food Interdisciplinary Science, School of Food Science and Technology, Dalian Polytechnic University, Dalian 116034 Liaoning, China;* orcid.org/0000-0003-0338-4364; Email: wanght6@foxmail.com, wanght@dlpu.edu.cn

Authors

Hongliang Li − *State Key Lab of Marine Food Processing & Safety Control, Dalian Polytechnic University, Dalian 116034 Liaoning, China; National Engineering Research Center of Seafood, Collaborative Innovation Center of Seafood Deep Processing, Nutrition and Health Food Pilot Base of Liaoning Dalian, and Academy of Food Interdisciplinary Science, School of Food Science and Technology, Dalian Polytechnic University, Dalian 116034 Liaoning, China; College of Food Science and Engineering, Jilin Agricultural University, Changchun 130118, P. R. China;* orcid.org/0000-0002-9291-4357

Hongjin Yu − *State Key Lab of Marine Food Processing & Safety Control, Dalian Polytechnic University, Dalian 116034 Liaoning, China; National Engineering Research Center of Seafood, Collaborative Innovation Center of Seafood Deep Processing, Nutrition and Health Food Pilot Base of Liaoning Dalian, and Academy of Food Interdisciplinary Science, School of Food Science and Technology, Dalian Polytechnic University, Dalian 116034 Liaoning, China*

Wentao Su − *State Key Lab of Marine Food Processing & Safety Control, Dalian Polytechnic University, Dalian 116034 Liaoning, China; National Engineering Research Center of Seafood, Collaborative Innovation Center of Seafood Deep Processing, Nutrition and Health Food Pilot Base of Liaoning Dalian, and Academy of Food Interdisciplinary Science, School of Food Science and Technology, Dalian Polytechnic University, Dalian 116034 Liaoning, China;* orcid.org/0000-0002-5233-1093

Mingqian Tan − *State Key Lab of Marine Food Processing & Safety Control, Dalian Polytechnic University, Dalian 116034 Liaoning, China; National Engineering Research Center of Seafood, Collaborative Innovation Center of Seafood Deep Processing, Nutrition and Health Food Pilot Base of Liaoning Dalian, and Academy of Food Interdisciplinary Science, School of Food Science and Technology, Dalian Polytechnic University, Dalian 116034 Liaoning, China;* orcid.org/0000-0002-7535-0035

Complete contact information is available at: https://pubs.acs.org/10.1021/acsomega.3c05542

Notes

The authors declare no competing financial interest.

■ ACKNOWLEDGMENTS

This work was supported by the National Natural Science Foundation of China, China (32372244) and Natural Science Foundation of Liaoning Province, China (2022-MS-347).

■ REFERENCES

(1) Yao, Q.; Ma, J.; Chen, X.; Zhao, G.; Zang, J. A natural strategy for astaxanthin stabilization and color regulation: Interaction with proteins. *Food Chem.* **2023**, *402*, 134343.

(2) Zhao, T.; Yan, X.; Sun, L.; Yang, T.; Hu, X.; He, Z.; Liu, F.; Liu, X. Research progress on extraction, biological activities and delivery systems of natural astaxanthin. *Trends Food Sci. Technol.* **2019**, *91*, 354−361.

(3) Tan, Y.; Zhou, H.; Zhang, Z.; McClements, D. J. Bioaccessibility of oil-soluble vitamins (A, D, E) in plant-based emulsions: impact of oil droplet size. *Food Funct.* **2021**, *12*, 3883−3897.

(4) Zhang, Y.; Wang, H.; Hou, Y.; Song, J.; Shang, W.; Zhang, P.; Hou, S.; Tan, M. Pickering emulsion stabilized by gliadin nanoparticles for astaxanthin delivery. *J. Food Eng.* **2023**, *345*, 111417.

(5) Onodera, T.; Kuriyama, I.; Andoh, T.; Ichikawa, H.; Sakamoto, Y.; Lee-Hiraiwa, E.; Mizushina, Y. Influence of particle size on the in vitro and in vivo anti-inflammatory and anti-allergic activities of a curcumin lipid nanoemulsion. *Int. J. Mol. Med.* **2015**, *35*, 1720−1728.

(6) Tan, Y.; Zhou, H.; McClements, D. J. Application of static in vitro digestion models for assessing the bioaccessibility of hydrophobic bioactives: A review. *Trends Food Sci. Technol.* **2022**, *122*, 314−327.

(7) Noreen, S.; Hasan, S.; Ghumman, S. A.; Anwar, S.; Gondal, H. Y.; Batool, F.; Noureen, S. Formulation, Statistical Optimization, and In Vivo Pharmacodynamics of Cydonia oblonga Mucilage/Alginate Mucoadhesive Microspheres for the Delivery of Metformin HCl. *ACS Omega.* **2023**, *8*, 5925−5938.

(8) Fathordoobady, F.; Jarzębski, M.; Pratap-Singh, A.; Guo, Y.; Abd-Manap, Y. Encapsulation of betacyanins from the peel of red dragon fruit (Hylocereus polyrhizus L.) in alginate microbeads. *Food Hydrocolloids* **2021**, *113*, 106535.

(9) Niizawa, I.; Espinaco, B. Y.; Zorrilla, S. E.; Sihufe, G. A. Natural astaxanthin encapsulation: Use of response surface methodology for the design of alginate beads. *Int. J. Biol. Macromol.* **2019**, *121*, 601−608.

(10) Zhang, C.; Xu, Y.; Wu, S.; Zheng, W.; Song, S.; Ai, C. Fabrication of astaxanthin-enriched colon-targeted alginate microspheres and its beneficial effect on dextran sulfate sodium-induced ulcerative colitis in mice. *Int. J. Biol. Macromol.* **2022**, *205*, 396−409.

(11) Zhang, X.; Zhao, X.; Tie, S.; Li, J.; Su, W.; Tan, M. A smart cauliflower-like carrier for astaxanthin delivery to relieve colon inflammation. *J. Controlled Release* **2022**, *342*, 372−387.

(12) Sadeghi, D.; Solouk, A.; Samadikuchaksaraei, A.; Seifalian, A. M. Preparation of internally-crosslinked alginate microspheres: Optimization of process parameters and study of pH-responsive behaviors. *Carbohydr. Polym.* **2021**, *255*, 117336.

(13) Leong, J.-Y.; Lam, W.-H.; Ho, K.-W.; Voo, W.-P.; Lee, M. F.-X.; Lim, H.-P.; Lim, S.-L.; Tey, B.-T.; Poncelet, D.; Chan, E.-S. Advances in fabricating spherical alginate hydrogels with controlled particle designs by ionotropic gelation as encapsulation systems. *Particuology* **2016**, *24*, 44−60.

(14) Paiboon, N.; Surassmo, S.; Rungsardthong Ruktanonchai, U.; Kappl, M.; Soottitantawat, A. Internal gelation of alginate microparticle prepared by emulsification and microfluidic method: Effect of Ca-EDTA as a calcium source. *Food Hydrocolloids* **2023**, *141*, 108712.

(15) Wang, P.; Li, M.; Wei, D.; Ding, M.; Tao, L.; Liu, X.; Zhang, F.; Tao, N.; Wang, X.; Gao, M.; Zhong, J. Electrosprayed Soft Capsules

of Millimeter Size for Specifically Delivering Fish Oil/Nutrients to the Stomach and Intestines. *ACS Appl. Mater. Interfaces* **2020**, *12*, 6536−6545.
(16) Saud, K. T.; Xu, J.; Wilkanowicz, S.; He, Y.; Moon, J. J.; Solomon, M. J. Electrosprayed microparticles from inulin and poly(vinyl) alcohol for colon targeted delivery of prebiotics. *Food Hydrocolloids* **2023**, *140*, 108625.
(17) Fani, N.; Enayati, M. H.; Rostamabadi, H.; Falsafi, S. R. Encapsulation of bioactives within electrosprayed kappa-carrageenan nanoparticles. *Carbohydr. Polym.* **2022**, *294*, 119761.
(18) Tao, L.; Xu, J.; Chen, J.; Liu, L.; Zhang, T.; Tao, N.; Wang, X.; Zhong, J. Preparation and characterization of internal gelation-based electrosprayed multicore millimeter-sized fish oil-loaded calcium alginate-stabilized capsules. *Food Hydrocolloids* **2022**, *128*, 107599.
(19) Yan, J.; Liang, X.; Ma, C.; McClements, D. J.; Liu, X.; Liu, F. Design and characterization of double-cross-linked emulsion gels using mixed biopolymers: Zein and sodium alginate. *Food Hydrocolloids* **2021**, *113*, 106473.
(20) Gómez-Mascaraque, L. G.; Perez-Masiá, R.; González-Barrio, R.; Periago, M. J.; López-Rubio, A. Potential of microencapsulation through emulsion-electrospraying to improve the bioaccesibility of β-carotene. *Food Hydrocolloids* **2017**, *73*, 1−12.
(21) Yu, H.; Wang, H.; Su, W.; Song, Y.; Zaky, A. A.; Abd El-Aty, A. M.; Tan, M. Co-delivery of hydrophobic astaxanthin and hydrophilic phycocyanin by a pH-sensitive water-in-oil-in-water double emulsion-filled gellan gum hydrogel. *Food Hydrocolloids* **2022**, *131*, 107810.
(22) Song, J.; Li, H.; Shang, W.; Wang, H.; Tan, M. Fabrication and characterization of Pickering emulsion gels stabilized by gliadin/starch complex for the delivery of astaxanthin. *Food Hydrocolloids* **2023**, *137*, 108388.
(23) Takatani, N.; Beppu, F.; Yamano, Y.; Maoka, T.; Miyashita, K.; Hosokawa, M. Preparation of Apoastaxanthinals and Evaluation of Their Anti-inflammatory Action against Lipopolysaccharide-Stimulated Macrophages and Adipocytes. *ACS Omega* **2022**, *7*, 22341−22350.
(24) Lama, A.; Provensi, G.; Amoriello, R.; Pirozzi, C.; Rani, B.; Mollica, M. P.; Raso, G. M.; Ballerini, C.; Meli, R.; Passani, M. B. The anti-inflammatory and immune-modulatory effects of OEA limit DSS-induced colitis in mice. *Biomed. Pharmacother.* **2020**, *129*, 110368.
(25) Ma, L.; Ni, L.; Yang, T.; Mao, P.; Huang, X.; Luo, Y.; Jiang, Z.; Hu, L.; Zhao, Y.; Fu, Z.; Ni, Y. Preventive and Therapeutic Spermidine Treatment Attenuates Acute Colitis in Mice. *J. Agric. Food Chem.* **2021**, *69*, 1864−1876.
(26) Chen, Y.; Su, W.; Tie, S.; Cui, W.; Yu, X.; Zhang, L.; Hua, Z.; Tan, M. Orally deliverable sequence-targeted astaxanthin nanoparticles for colitis alleviation. *Biomaterials* **2023**, *293*, 121976.
(27) Mehregan Nikoo, A.; Kadkhodaee, R.; Ghorani, B.; Razzaq, H.; Tucker, N. Controlling the morphology and material characteristics of electrospray generated calcium alginate microhydrogels. *J. Microencapsulation* **2016**, *33*, 605−612.
(28) Kim, E. S.; Baek, Y.; Yoo, H. J.; Lee, J. S.; Lee, H. G. Chitosan-Tripolyphosphate Nanoparticles Prepared by Ionic Gelation Improve the Antioxidant Activities of Astaxanthin in the In Vitro and In Vivo Model. *Antioxidants* **2022**, *11*, 479.
(29) Gu, L.; Ji, S.; Wu, B.; Wang, W.; Cheng, J.; Xia, Q. Astaxanthin encapsulation in nanocapsule by high-pressure homogenization technology: a study on stability, antioxidant activity and in vitro release. *J. Dispersion Sci. Technol.* **2023**, 1−12.
(30) Lima, D. S.; Tenório-Neto, E. T.; Lima-Tenório, M. K.; Guilherme, M. R.; Scariot, D. B.; Nakamura, C. V.; Muniz, E. C.; Rubira, A. F. pH-responsive alginate-based hydrogels for protein delivery. *J. Mol. Liq.* **2018**, *262*, 29−36.
(31) Wang, K.; Ni, J.; Li, H.; Tian, X.; Tan, M.; Su, W. Survivability of probiotics encapsulated in kelp nanocellulose/alginate microcapsules on microfluidic device. *Food Res. Int.* **2022**, *160*, 111723.
(32) Yang, J.; Hua, S.; Huang, Z.; Gu, Z.; Cheng, L.; Hong, Y. Comparison of bioaccessibility of astaxanthin encapsulated in starch-based double emulsion with different structures. *Carbohydr. Polym.* **2021**, *272*, 118475.
(33) Zhang, R.; Zhang, Z.; Zou, L.; Xiao, H.; Zhang, G.; Decker, E. A.; McClements, D. J. Enhancement of carotenoid bioaccessibility from carrots using excipient emulsions: influence of particle size of digestible lipid droplets. *Food Funct.* **2016**, *7*, 93−103.
(34) Zhen, D.; Xuan, T. Q.; Hu, B.; Bai, X.; Fu, D. N.; Wang, Y.; Wu, Y.; Yang, J.; Ma, Q. Pteryxin attenuates LPS-induced inflammatory responses and inhibits NLRP3 inflammasome activation in RAW264.7 cells. *J. Ethnopharmacol.* **2022**, *284*, 114753.
(35) Al-Tarifi, B. Y.; Mahmood, A.; Sheikh, H. I.; Wan Ahmad, W. A. N.; Assaw, S. Inhibitory Effects of Astaxanthin on Lps-Induced Raw 264.7 Inflammation and Breast Cancer Mcf-7 Cell Lines Proliferation. *J. Sustainability Sci. Manage.* **2022**, *17*, 55−66.
(36) Liang, Y.; Zha, S.; Tentaku, M.; Okimura, T.; Jiang, Z.; Ueno, M.; Hirasaka, K.; Yamaguchi, K.; Oda, T. Suppressive effects of sulfated polysaccharide ascophyllan isolated from Ascophyllum nodosum on the production of NO and ROS in LPS-stimulated RAW264.7 cells. *Biosci., Biotechnol., Biochem.* **2021**, *85*, 882−889.
(37) Deng, J.; Zhao, L.; Yuan, X.; Li, Y.; Shi, J.; Zhang, H.; Zhao, Y.; Han, L.; Wang, H.; Yan, Y.; Zhao, H.; Wang, H.; Zou, F. Pre-Administration of Berberine Exerts Chemopreventive Effects in AOM/DSS-Induced Colitis-Associated Carcinogenesis Mice via Modulating Inflammation and Intestinal Microbiota. *Nutrients* **2022**, *14*, 726.
(38) Wei, C.; Wang, J.-Y.; Xiong, F.; Wu, B.-H.; Luo, M.-H.; Yu, Z.-C.; Liu, T.-T.; Li, D.-F.; Tang, Q.; Li, Y.-X.; Zhang, D.-G.; Xu, Z.-L.; Jin, H.-T.; Wang, L.-S.; Yao, J. Curcumin ameliorates DSSinduced colitis in mice by regulating the Treg/Th17 signaling pathway. *Mol. Med. Rep.* **2021**, *23*, 34.
(39) Liang, L.; Xiong, Q.; Kong, J.; Tian, C.; Miao, L.; Zhang, X.; Du, H. Intraperitoneal supplementation of iron alleviates dextran sodium sulfate-induced colitis by enhancing intestinal barrier function. *Biomed. Pharmacother.* **2021**, *144*, 112253.
(40) Li, Y.; Pan, X.; Yin, M.; Li, C.; Han, L. Preventive Effect of Lycopene in Dextran Sulfate Sodium-Induced Ulcerative Colitis Mice through the Regulation of TLR4/TRIF/NF-κB Signaling Pathway and Tight Junctions. *J. Agric. Food Chem.* **2021**, *69*, 13500−13509.
(41) Zhang, X.; Zhao, X.; Hua, Z.; Xing, S.; Li, J.; Fei, S.; Tan, M. ROS-triggered self-disintegrating and pH-responsive astaxanthin nanoparticles for regulating the intestinal barrier and colitis. *Biomaterials* **2023**, *292*, 121937.
(42) Zheng, W.; Song, H.; Luo, Z.; Wu, H.; Chen, L.; Wang, Y.; Cui, H.; Zhang, Y.; Wang, B.; Li, W.; Liu, Y.; Zhang, J.; Chu, Y.; Luo, F.; Liu, J. Acetylcholine ameliorates colitis by promoting IL-10 secretion of monocytic myeloid-derived suppressor cells through the nAChR/ERK pathway. *Proc. Natl. Acad. Sci. U.S.A.* **2021**, *118*, 118.
(43) Affandi, M. M. M.; JuLianto, T.; maJeed, A. B. A. Enhanced oral bioavailability of astaxanthin with droplet size reduction. *Food Sci. Technol. Res.* **2012**, *18* (4), 549−554.

https://doi.org/10.1021/acsomega.3c05542
ACS Omega 2023, 8, 41537−41547